High-Power Multicell Interleaved Flyback Converter for Design of Intercell Transformers

Dr.ECCLESTON
Assistant Professor, Dept of EEE
Christu Jyoti Institute of Technology and Science
Jangaon,Telangana,India

PROF.MUSILEK
Mtech Scholar
Vaagdevi College of Engineering
Warangal,Telangana,India

Abstract:This paper presents the developments and the results of an analytic method elaborated to design isolated intercell transformers. These particular magnetic components are intended for multicell interleaved flyback converters recently proposed and well-suited to low-voltage, high-power applications. A specific 2-D model to evaluate the winding losses is included in the design pro-cess. The results, obtain for standard core shapes, allow defining the ranges of the main parameters, number of cells, and switching frequency, required for future realizations.

Index Terms:—Flyback converter, intercell transformer (ICT),interleaved converters, interphase transformers.

I. INTRODUCTION

Recently, an original multicell interleaved flyback con-verter using intercell transformers (ICT) was presented This topology shows some interesting characteristics that can be used when a modular design is desired. The simplicity of the elementary cell, the large duty cycle control capability in case of variations of input dc voltage, and the good transient behavior as a result of the ICT properties are the main advan-tages. Nevertheless, these converters still need to be compared with more standard designs (interleaved push–pull or bridges). Unfortunately, the number of cells required to provide good op-erating conditions is high (typically greater than six to seven), and consequently, the realization of demonstrative prototypes is critical. This difficulty is strengthened by the particular behavior of ICT and by many subcases related to the number of cell (even or odd, multiple of four or not. . .). Therefore, before any pro-totype is constructed, it is essential to determine, as accurately as possible, the feasible ICT topologies and their characteristics (losses, volumes, and winding arrangements) in correlation with the number of cells.

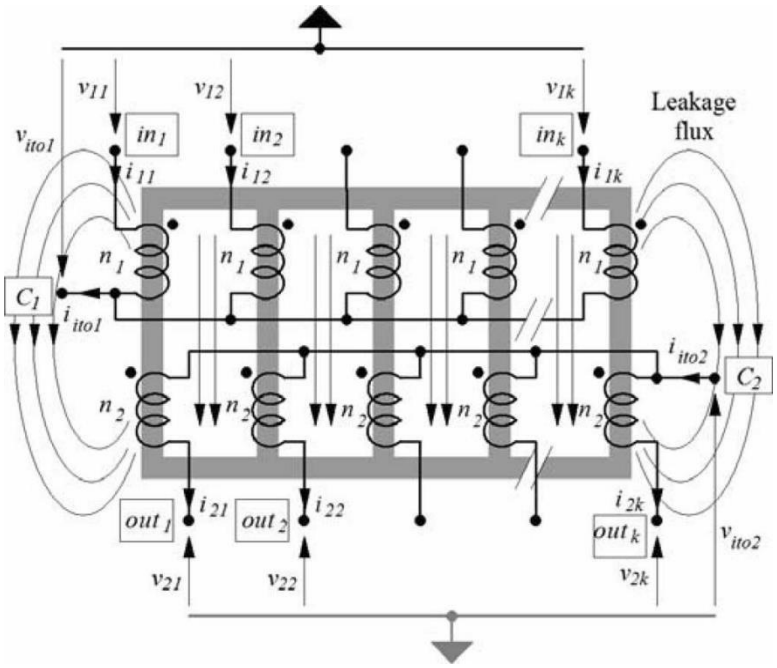

Fig. 1. Two-side monolithic ICT.

To reach this goal, and after some review of the operation of the ICT flyback converter, the first part of the paper is ded-icated to the winding loss estimation in an ICT cell, with the introduction of a 2-D model compatible with the particular cur-rent distributions encountered in these devices. The following part describes the design method specifically elaborated for the ICT that includes the previous model. The last part presents the design of a representative ICT. It shows the mains quantitative tendencies concerning number of cells or efficiency and finally gives useful data for future realizations.

ICT FLYBACK CONVERTER

A. Topology

In this part, the main characteristics of the ICT flyback converter, more precisely described in [1], are reviewed. The ICT flyback converter uses the isolated ICT concept, of which an example using a monolithic core is given in Fig. 1. The ICTs can be built with various magnetic core shapes, the as-sociation of separate transformers being a classic way of de-sign [2], [4]–[6], [8]–[10], and corresponding isolated ICTs can be derived.

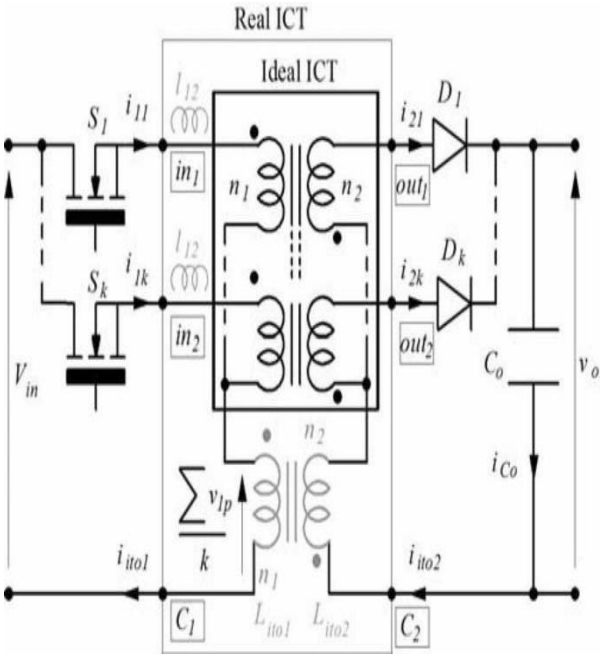

Fig. 2. ICT flyback converter

If the shape is symmetrical, the general equations of the iso-lated ICTs are [1], [4]

$$v_{ito1} = \frac{\sum_{p=1}^{k} v_{1p}}{k} - L_{ito1}\frac{di_{ito1}}{dt} - M\frac{di_{ito2}}{dt} - l_{12}\frac{di_{ito1}}{dt} \quad (1)$$

$$v_{ito2} = \frac{\sum_{p=1}^{k} v_{2p}}{k} - M\frac{di_{ito1}}{dt} - L_{ito2}\frac{di_{ito2}}{dt} - l_{12}\frac{di_{ito2}}{dt} \quad (2)$$

where $i_{ito1} = \sum_{p=1}^{k} i_{1p}$ and $i_{ito2} = \sum_{p=1}^{k} i_{2p}$.

In this model and throughout the paper, the magnetizing in-ductances are neglected, because the magnetizing currents are generally negligible compared with the main currents and have no impact on the general properties of the ICTs presented here.

1) L_{ito1}, L_{ito2}correspond to the sum of the fluxes generated,respectively, by the k primary windings and by the k sec-ondary windings and circulating in the air, in the topology of Fig. 1.
2) M corresponds to the sum of the k fluxes common tothe primary and secondary windings of each cell. In the topology of Fig. 1, the return path for the sum of these k fluxes is in the air.
3) $l_{12}$is the leakage inductance that corresponds to the leak-age flux between the two windings of each cell (also in the air).

The method to express the different inductances is developed in [1].

An ideal ICT could be defined considering Fig. 1 by neglect-ing the fluxes in the air. In that case, this ideal ICT realizes a perfect voltage conversion, as in a classical ideal transformer, described by (1) and (2) with $L_{ito1}=L_{ito2}=M=l_{12}= 0$, completed by the k relations $v_{2p}=n_2/n_1 v_{1p}$, $p= 1, \ldots, k$. However, such an ICT would not store any energy and flyback operation would not be allowed.

The basic topology of the ICT flyback converter is given in Fig. 2. It includes the ICT (that is represented by the ideal part de-fined earlier to which are added the air-coupled inductor (L_{ito1} , L_{ito2} , M) and the leakage inductors l_{12}, k primary switches, k secondary diodes, and a single-output capacitor [here v_{ito1} and$v_{ito2}$are null in (1) and (2)]. If the control sequences of the k switches are interleaved, the frequency of the voltage applied to the equivalent coupled-inductor is kF, the switching frequency of each cell being F , and the amplitude is divided by k.

With a high number of cells (>6), the energy stored in the air-coupled inductance (L_{ito1} , L_{ito2}, M) is sufficient for flyback operation. Therefore, the behavior of the ICT is very close to a classical transformer, and no air-gap is needed.

The scheme shown in Fig. 2 can also be realized with common source switches to make the design easier. The effect of connec-tions can be included in the inductances l_{12} . They constitute a drawback for the turn-off switching as in a classical single-stage flyback converter, but conversely, they have a positive impact on the total current ripple.

In [1], the evolution of the ripple current in that topology has been calculated.

$$\Delta i_{ito} = \frac{[kD - q + 1]\,[q - kD]}{1 - D}\,\frac{V_{\text{in}}}{k^2 L_{ito1} F}$$

$$i_{ito} = i_{ito1} + \frac{n_2}{n_1} i_{ito2}. \quad (3)$$

The design of ICTs, with realistic values of the current rip-ple (20%–50%), based on a parametric study considering both variables F and k, will be the first aim of this paper.

B. Properties

To realize dc–dc converters with input voltage $V_{\text{in}}<$ 50 V, and output power $P >$ 5 kW, designers widely use parallel associations of cells, because of the high cur-rent values [1], [7], [11], [22]. It is often preferred to di-rectly parallelize the switches. Then, the interleaving con-trol is a logical step forward to improve filter design and dynamic behavior. The ICT flyback converter seems to be a good candidate in that context with the following properties.

1) The basic cell is very simple but does not suffer the main drawback of the classic flyback converter, i.e., the low efficiency of the coupled inductor.
2) The ICT topology provides a very good dynamic behavior in regulation, because of the very low output inductance [8].
3) The flyback converter topology is interesting in case of large variations of input dc voltage that frequently occur in low-voltage applications. Indeed, the duty cycle can exceed 0.5, allowing an easy adaptation to the lower volt-age of the input dc range. Therefore, the optimal 0.5 duty cycle can be maintained for the nominal operating point, avoiding the oversizing suffered by direct converters such as full-bridge, forward, or push–pull under the same con-ditions.
4) In the balanced ICT, the dc currents generate very low dc magnetic flux [4]; consequently, the topology is not really sensitive to magnetic saturation effects in case of high current transients.

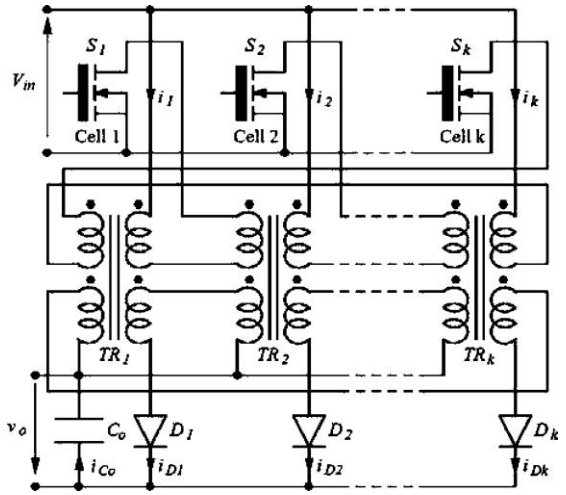

Fig. 3. ICT flyback converter using "cyclic cascade" association of transformers.

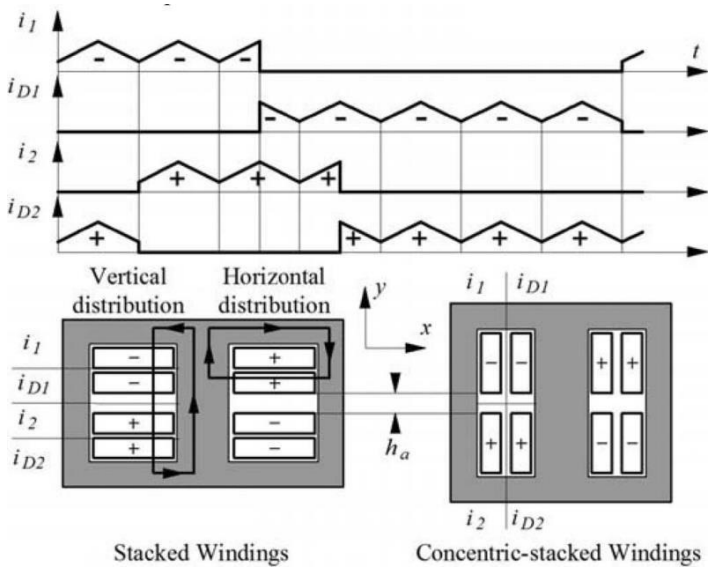

Fig. 4. Current distributions in the windings of ICT.

BI.TOPOLOGY AND DESIGN PROBLEM OF ICT

A. Topology of ICT

As has been shown in [2]–[4], various shapes of ICTs can be considered, which go from monolithic designs that should theoretically reach high power density but are difficult to realize, to various associations of separate transformers.

The authors currently evaluate different options but one par-ticular association, known as "cyclic-cascade" is really modular and seems to be a good solution, if the permutated control mode described in [4] is applied. The ICT flyback converter scheme as-sociated with the cyclic-cascade configuration is given in Fig. 3. It uses k separate and identical transformers, each of them in-cluding two primary and two secondary windings. The design methodology presented here is based on this configuration.

B. Problem of Magnetic Design

If the behavior of ICT is close to that of classic transformers (it is particularly true for the single-side topologies used in nonisolated converters), some specificities have to be considered in the evaluation of the losses required by any design approach (core and winding losses).

1) Conductor Losses: In any transformer of Fig. 3, the cur-

rents of the primary and secondary windings flow between two adjacent cells. Fig. 4 shows the current distribution in TR_2 ; the distribution in any other transformer can be derived by circular permutation. It leads to a specific electromagnetic configuration in the window, particularly in the case of concentric-stacked windings.

The stacked configuration should be preferred for planar

transformers; the concentric-stacked configuration for ETD core or similar types. In both cases, a space h_a is introduced between the two winding groups, to adjust the inductances L_{ito} . The leak-age inductances l_{12} (see Fig. 2) depend on the space be

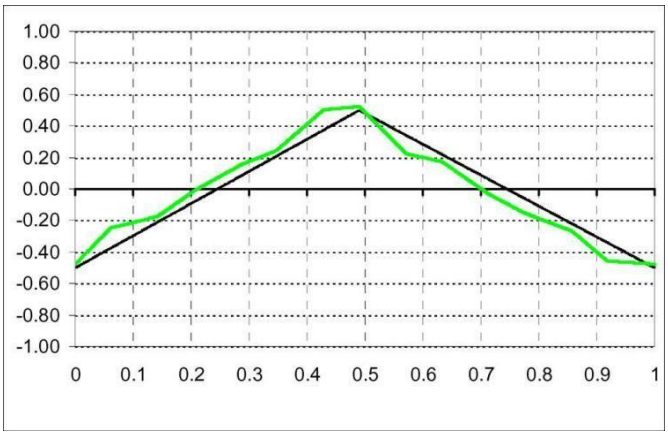

Fig. 5. Magnetic field shape in ICTs.

the two windings of the same group and these are required to be as close as possible.

In the stacked configuration, the amp-turns enlaced by an arbi-trary path flowing vertically through the window (vertical distri-bution of Fig. 4) are null because the sum $i_1+i_{D1}+i_2+i_{D2}$ is zero at any time of the switching period. Therefore, the magnetic field component H_y is also null in the window, as in a classical transformer. The problem is still a monodimensional one, but with particular distribution and waveforms of the currents in the windings.

In the concentric-stacked configuration, which provides high values of inductances L_{ito} , the ampere-turns are nonnull in the two directions; therefore, the magnetic field repartition is bidimensionnal. Consequently, the evaluation of winding losses needs a bidimensional model.

2) Magnetic Losses: As demonstrated in [4], the magneticfield in the ICT cores does not have the triangular or trapezoidal shapes observed in classical transformers. Fig. 5 shows a typical field shape generated in one transformer core of the cyclic-cascade association, in permutated mode and for a duty cycle value of 0.5.

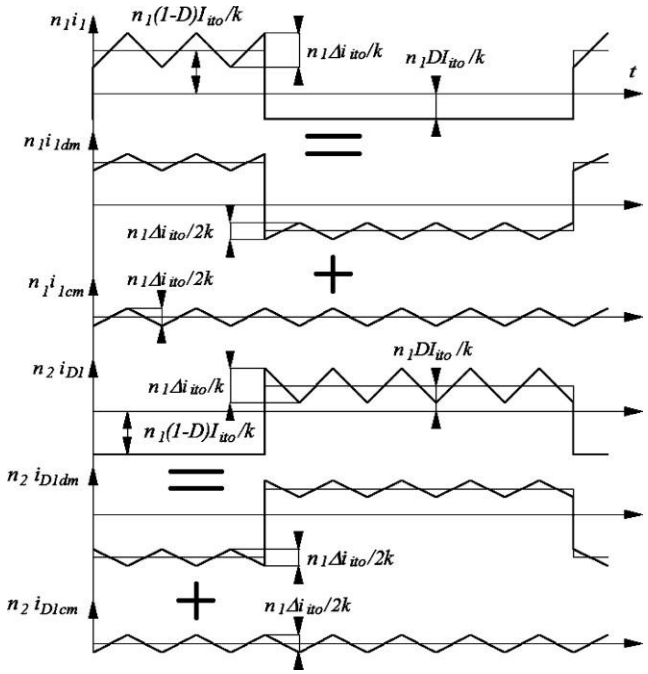

Fig. 6. Decomposition of the currents.

For this operating point, the flux waveform is very close to the triangle and the core losses are similar to a sinusoidal excitation of the same amplitudes. The measurements made in [1] confirm this approximation and sinusoidal loss models will be used in the design in the last section.

C. 2-D Analytical Model for Conductor Losses

The previous section had emphasized the need for a bidi-mensional model to estimate the winding losses. Such a model can be achieved by splitting up the problem in two monodi-mensional approaches. Indeed, each of the winding currents can be separated into two components, resulting in a common mode ($index_{cm}$) and a differential mode ($index_{d\,m}$). Fig. 6 shows the decomposition for the first winding group of the transformer TR_2, without the dc components. The common-mode amp-turns are identical in both windings and the differential amp-turns are opposite, which brings

$$n_1 i_{1dm} = -n_2 i_{2D1dm} \text{ and } n_1 i_{1cm} = n_2 i_{2D1cm} = n_1 i_{1cm}.$$

The separating method can be applied to the two typical con-figurations of Fig. 4. The repartition of both modes in the wind-ings is illustrated in Fig. 7 (only the left window is represented).
Stacked Configuration: In this case, the common and dif-ferential modes generate a monodimensional magnetic field H_x. For the differential mode, each winding group operates as the two windings of a classical transformer ($+n_1 i_{1d\,m}$, $-n_1 i_{1d\,m}$ then $+n_2 i_{2d\,m}$, $-n_2 id_{2d\,m}$), and for the common mode, as the primary ($-n_1 i_{c\,m}$, $-n_1 id_{c\,m}$) or the secondary ($+n_1 i_{c\,m}$, $+n_1 id_{c\,m}$) of a classical transformer. The well known 1-D an-alytic model [12]–[15] can be applied in the two modes and superposing the results gives the total winding losses.

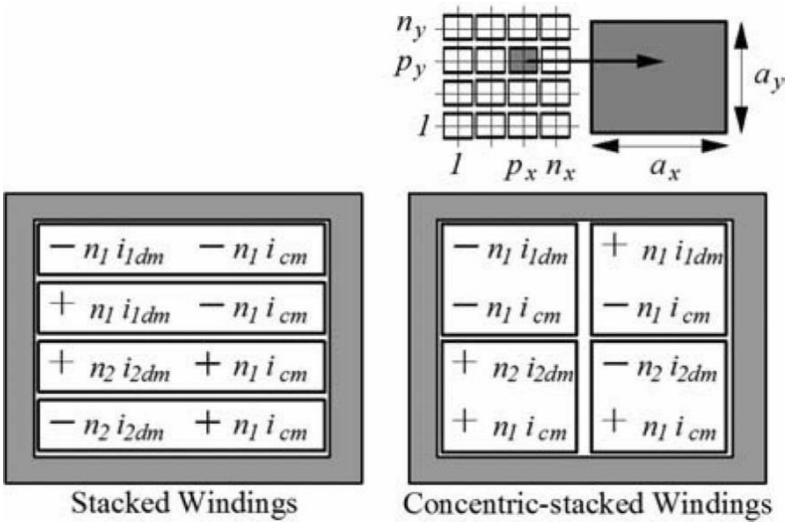

Fig. 7. Repartition of the common and differential modes in the windings

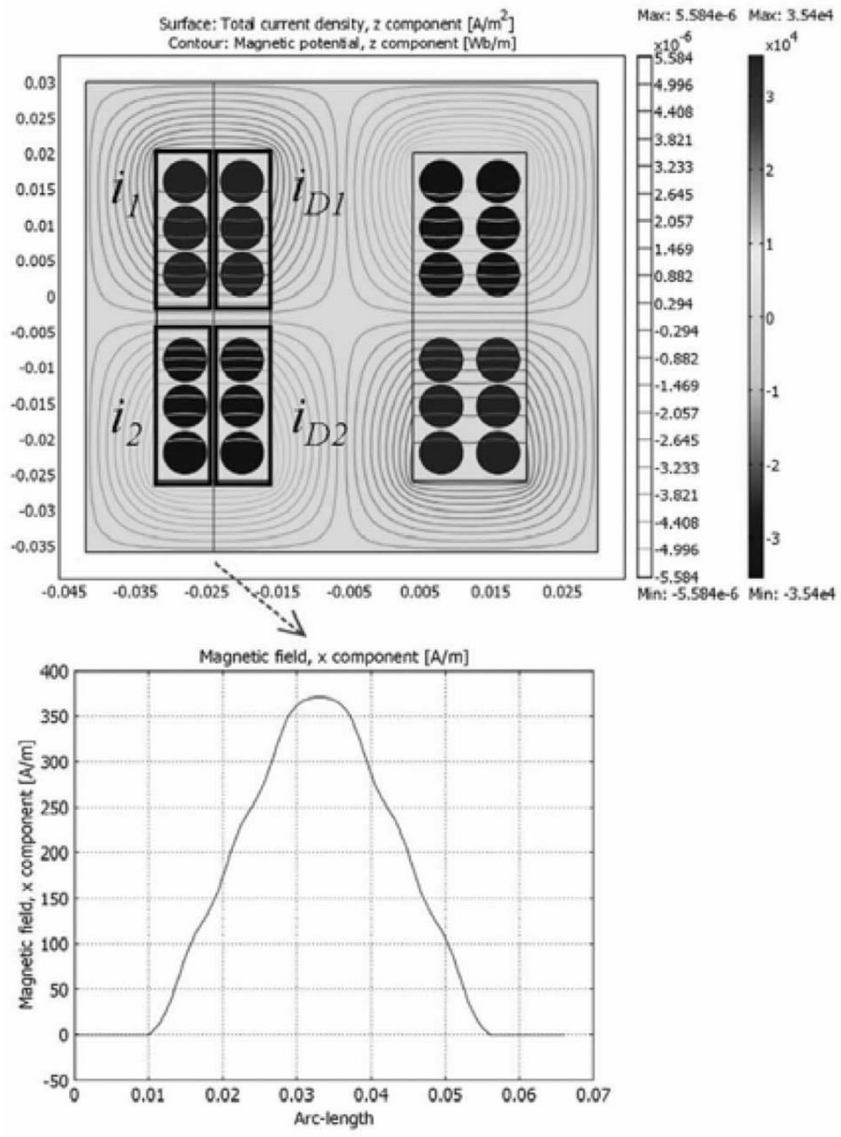

Fig. 8. Magnetic field distribution for the common mode.

2) Concentric-Stacked Configuration: As in the previous

case, the common mode generates a monodimensional mag-netic field H_x (see finite-element (FE) simulation of Fig. 8), and the analytic calculus will be the same for that component.

For the differential mode, the concentric-stacked configu-

ration is more complicated. The four differential components ($+n_1 i_{1d\,m} - n_1 i_{d1d\,m} + n_2 i_{2d\,m} - n_2 i_{d2d\,m}$) create a bidimen-sional magnetic field and the problem remains a bidimensional problem. It can be solved by introducing an approximation: If the permutated control mode is used, the phase between the

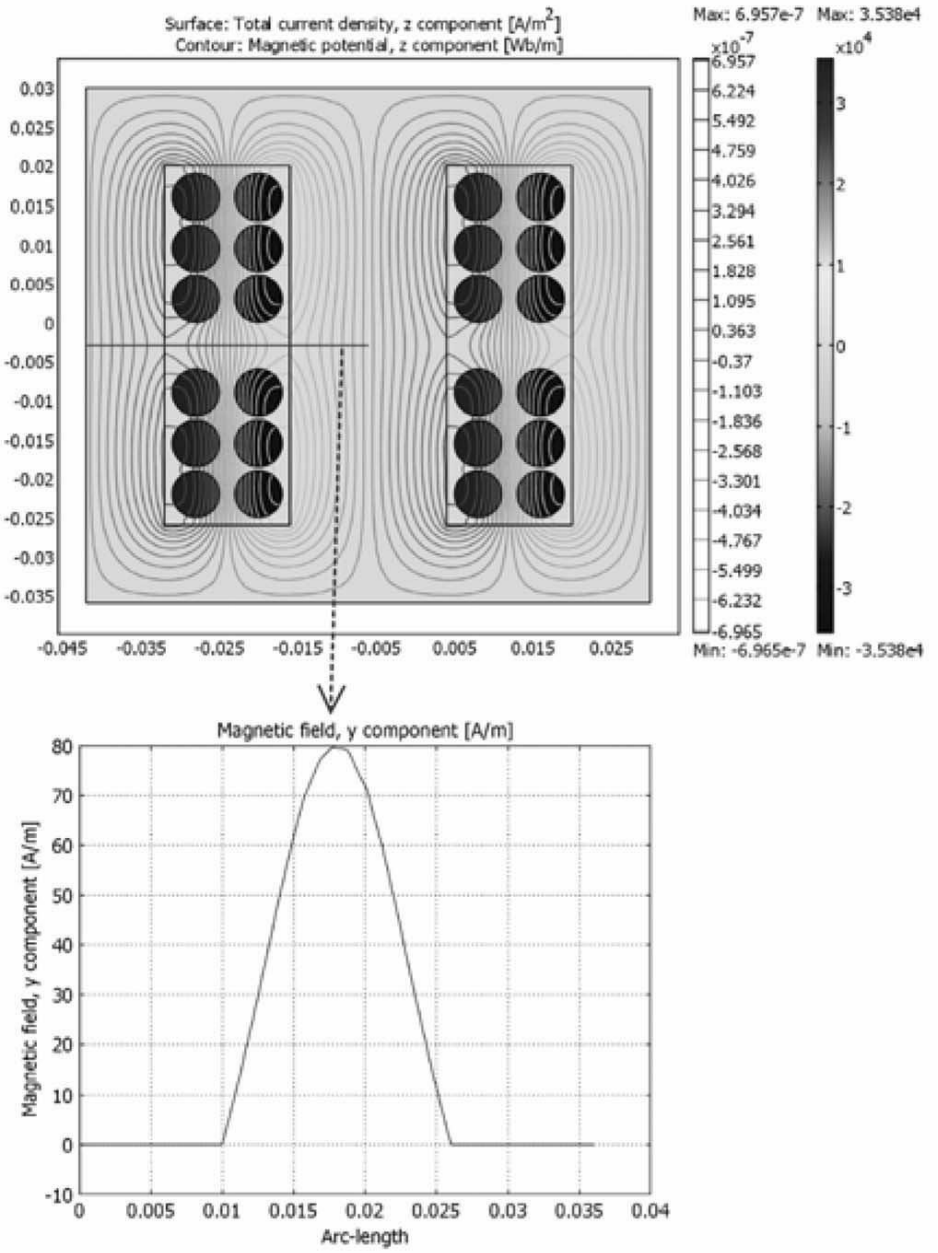

Fig. 9. Approximate magnetic field distribution for the differential mode.

currents $i_{1d\,m}$ and $i_{2d\,m}$ is close to 180° for the high value of k [4]. Therefore, it can be considered that $n_1 i_{1d\,m} \approx -n_2 i_{2d\,m}$, and a transformer configuration appears in the verticaldimension.

This is illustrated by the FE simulation in Fig. 9. To complete this analysis, other FE simulations have been made for different values of the phase between $n1i1dm$ and $n2i2dm$ (160°–200°). They show that the approximation is correct, and that the ad-ditional winding losses because of the missing component are negligible.

The analytic formulation can now be deduced from the pre-vious qualitative analysis. Each winding includes $nx \times ny$ rect-angular conductors (see Fig. 7). A geometrical transformation has to be made in case of circular conductors. By summing the common and differential modes for each harmonic component of the currents (row h), the expression of winding losses $Pw\text{-}xy$ in a conductor placed in the line py and in the column $x\,px$ is

$$P_{w\text{-}xy} = R_{DC\text{-}xy} \times \left[\begin{array}{l} \left[\begin{array}{l} (2p_x^2 - 2p_x + 1)\Delta_x F_1(\Delta_x) \\ -4p_x(p_x - 1)\Delta_x F_2(\Delta_x) \end{array} \right] \underline{I_{dmh}} \underline{I^*_{dmh}} \\ + \left[\begin{array}{l} (2p_y^2 - 2p_y + 1)\Delta_y F_1(\Delta_y) \\ -4p_y(p_y - 1)\Delta_y F_2(\Delta_y) \end{array} \right] \underline{I_{dmh}} \underline{I^*_{dmh}} \\ + R_e(\underline{I_{cmh}} \underline{I^*_{dmh}}) + R_e(\underline{I_{dmh}} \underline{I^*_{cmh}}) \end{array} \right].$$

With

$$\delta = \sqrt{\frac{\rho}{h\pi F \mu}}, \qquad \Delta_x = \frac{a_x}{\delta}, \qquad \Delta_y = \frac{a_y}{\delta}$$

$$F_1(\Delta) = \frac{\sinh(2\Delta) + \sin(2\Delta)}{\cosh(2\Delta) + \cos(2\Delta)}$$

$$F_2(\Delta) = \frac{\sinh(\Delta)\cos(\Delta) + \cosh(\Delta)\sin(\Delta)}{\cosh(2\Delta) - \cos(2\Delta)}$$

and *Idmh* being the complex current associated with the harmonic*h* of *idm* and *Icmh* the complexcurrent associated withthe harmonic *h* of *icm* .

By adding the contributions of all the conductors, for all theharmonic components, the total losses in the winding can beexpressed as

$$P_w = R_{\text{dctot}} I^2 \sum_{h=0}^{\infty} \times \left[\begin{array}{l} \left[\begin{array}{l} \frac{1}{3}(2n_x^2+1)\Delta_x F_1(\Delta_x) \\ -\frac{4}{3}(n_x^2-1)\Delta_x F_2(\Delta_x) \end{array} \right] \underline{I_{dmh}} \underline{I^*_{dmh}} / I^2_{\text{rms}} \\ + \left[\begin{array}{l} \frac{1}{3}(2n_y^2+1)\Delta_y F_1(\Delta_x) \\ -\frac{4}{3}(n_y^2-1)\Delta_y F_2(\Delta_x) \end{array} \right] \underline{I_{cmh}} \underline{I^*_{cmh}} / I^2_{\text{rms}} \\ + 2R_e(\underline{I_{cmh}} \underline{I^*_{dmh}}) / I^2_{\text{rms}} \end{array} \right].$$

with $R_{\text{d ctot}}$ as the dc winding resistor value and $I_{\text{rm s}}$ as the rms value of the winding current. Then, the ac resistor value can be

$$R_{\text{actot}} = R_{\text{dctot}} \sum_{h=0}^{\infty} \times \left[\begin{array}{l} \left[\begin{array}{l} \frac{1}{3}(2n_x^2+1)\Delta_x F_1(\Delta_x) \\ -\frac{4}{3}(n_x^2-1)\Delta_x F_2(\Delta_x) \end{array} \right] \underline{I_{dmh}} \underline{I^*_{dmh}} / I^2_{\text{rms}} \\ + \left[\begin{array}{l} \frac{1}{3}(2n_y^2+1)\Delta_y F_1(\Delta_x) \\ -\frac{4}{3}(n_y^2-1)\Delta_y F_2(\Delta_x) \end{array} \right] \underline{I_{cmh}} \underline{I^*_{cmh}} / I^2_{\text{rms}} \\ + 2R_e(\underline{I_{cmh}} \underline{I^*_{dmh}}) / I^2_{\text{rms}} \end{array} \right]$$

$$R_{\text{acot}} = R_{\text{dctot}}\, g(n_x, n_y, F).$$

IV. DESIGN OF ICTS

The general design method used in this section is more pre-cisely described in [15]. It is basedon the area product cal-culation [16], [17] of generic core shapes of which sizes varyaccording to a homothetic law (Fig. 10).

The considered core shapes correspond to standard families,planar or ETD types, very frequently used by the designers.

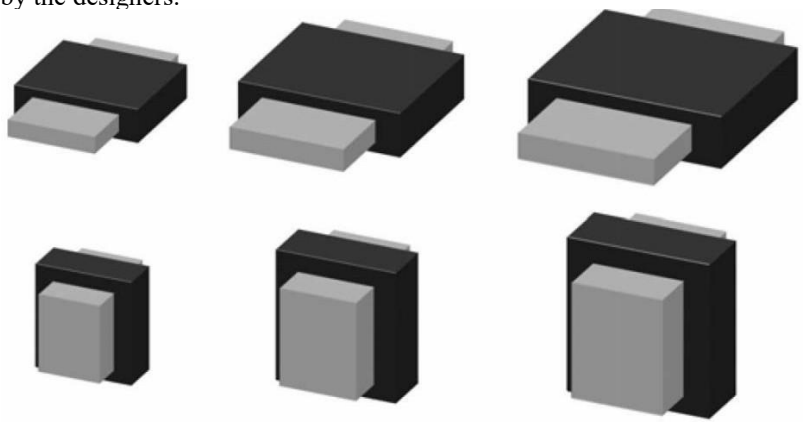

Fig. 10. Homothetic shapes.

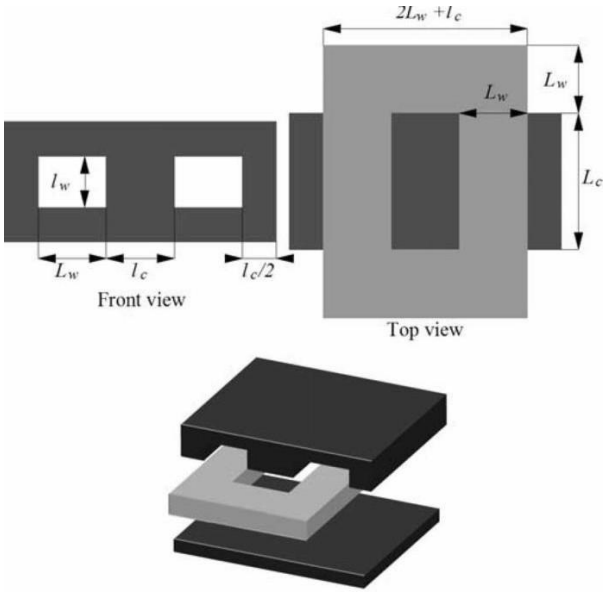

Fig. 11. Dimensional characteristics of the considered cores

geometrical parameters and associating the area product to the physical parameters of the transformer.

One of the most important parameters of the design is the temperature increase of the transformer [18]–[21]. Therefore, a correct evaluation of the core and winding losses is necessary, thus requiring the use of robust and realistic loss models.

The method is based on the solution of (4), available for a two-winding transformer or a four-winding transformer including two groups of identical windings (push–pull and ICT flyback converter). It can be easily extended to any number of windings.

By taking into account the temperature increase ΔT , corre-lated to the core and winding losses, the current densities $J_{1,2rms}$ and the maximal magnetic induction ΔB_M can be expressed by relations

$$A_w A_c = P \frac{\left[K_{P1} \frac{K_{w1}}{J_{1\mathrm{rms}}(A_w A_c)} + K_{P2} \frac{K_{w2}}{J_{2\mathrm{rms}}(A_w A_c)}\right]}{\Delta B_M (A_w A_c) F} \tag{4}$$

$$J_{1,2\mathrm{rms}}(A_w A_c) = \left[\frac{\Delta THS (A_w A_c)^{\frac{1}{2}}}{(1 + 2/\beta_F)\mathrm{Vol}_w g_{1,2}(n_{x1,2},\, n_{y1,2}, F)\rho}\right]^{\frac{1}{2}} \tag{5}$$

$$\text{with } \mathrm{Vol}_w = \left[\frac{1}{2K_{w1}} + \frac{1}{2K_{w2}}\right] Z (A_w A_c)^{3/4}$$

$$\Delta B_M (A_w A_c) = \left[\frac{\Delta THS (A_w A_c)^{\frac{1}{2}}}{\mathrm{Vol}_c (1 + \beta_F/2)(K_{c1} F^{\alpha 1} + K_{c2} F^{\alpha 2})}\right]^{\frac{1}{\beta_F}} \tag{6}$$

$$\text{with } \mathrm{Vol}_c = Y (A_w A_c)^{\frac{3}{4}}$$

$$A_c = \frac{K_E V_{\mathrm{in}}}{n_1 \Delta B_M F}. \tag{7}$$

Parameters:

P	transformer power;
ΔT	average temperature increase of the transformer;
H	thermal exchange coefficient;
S, Z, Y	geometrical parameters depending on the core shape and functions of the three following parameters: $a_w = L_w / l_w, \quad a_{c1} = L_c / l_w, \quad a_{c2} = l_c / l_w;$
K_{w1}, K_{w2}	winding coefficients, ratio window/ copper;
K_{P1}, K_{P2}	power coefficients depending on the converter topology;
$\alpha_1, \alpha_2, K_{c1}, K_{c2}, \beta_F$	parameters of the core loss model expressing precisely the core loss density P_c as a function of induction over a wider frequency range than the classic Steinmetz model [15]: $P_c = (K_{c1} F^{\alpha 1} + K_{c2} F^{\alpha 2}) \Delta B_M^{(\beta - a_B F)} = (K_{c1} F^{\alpha 1} + K_{c2} F^{\alpha 2}) \Delta B_M^{\beta_F};$ (8)
g_1, g_2	functions associated with the ac winding losses that define the global ratio $R_{\mathrm{ac}}/R_{\mathrm{dc}}$. They depend on the converter and winding topologies. In the present case, they are deduced from the results of Section III-C.

Intrinsically, the g functions also depend on the area product $A_w A_c$ as J_{rms} (5) and ΔB_M (6). Therefore, the two sides of (4) depend on $A_w A_c$, and finding the $A_w A_c$ value requires solving (4) that can be made by a zero search of (9)

$$A_w A_c - P \frac{\left[K_{P1} \frac{K_{w1}}{J_{1\mathrm{rms}}(A_w A_c)} + K_{P2} \frac{K_{w2}}{J_{2\mathrm{rms}}(A_w A_c)} \right]}{\Delta B_M (A_w A_c) F} = G(A_w A_c) = 0. \quad (9)$$

The calculation process of the area product using (9) will bemore precisely described in the next part (Fig. 12). It is based

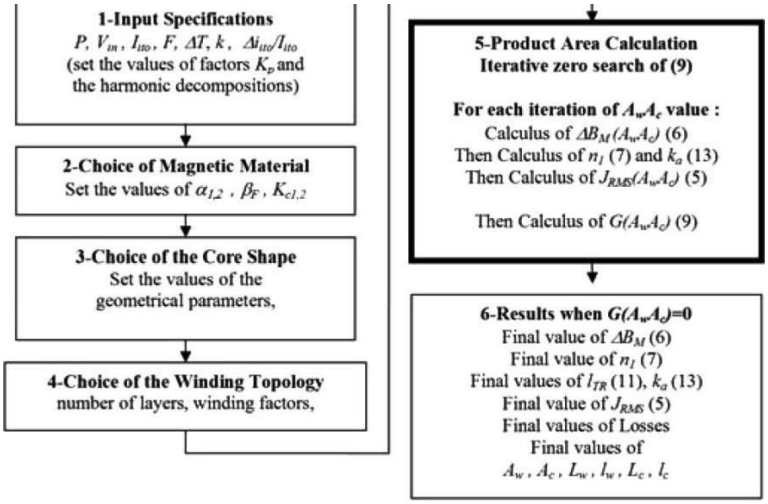

Fig. 12. Design process.

on the iterative calculation versus A_cA_w of ΔB_M (6), J_{rms} (5) until (9) is verified.

B. Specific Parts of Design for the ICT

1) Winding Losses: As shown in Section III-C, the application of the general method for the ICT needs a particularformulation for the winding losses.

2) Leakage Inductance: Another design element specific tothe ICT concept is the introduction of the inductance L_{ito} calculationthat fixes the ripple current in the ICT topology. It must beone of the input parameters of the design. In the separated transformertopology, it directly derives from the leakage inductancel_{TR} of the elementary transformer.Still considering the arrangements of Fig. 4, the interwindingspace h_a is defined as a proportion of l_w with

$$h_a = k_a\, l_w .$$

Then, the analytic expression of the leakage inductance forone of the k transformers is

$$\begin{aligned} l_{\mathrm{TR}} &= \mu_o n_1^2 \frac{k_a l_w}{L_w} 2(L_c + l_c + 2L_w) \\ &= \mu_o n_1^2 k_a l_w \frac{2(a_{c1} + a_{c2} + 2a_w)}{a_w}. \end{aligned} \qquad (10)$$

This expression neglects the field in the windings and givesan underestimated value taking into account only the magneticfield in the space h_a . That choice considerably simplifies thecalculation process (the winding part of the leakage inductancedepends on frequency as the resistance) with the slight consequenceof a real ripple a little lower than the calculated one.As the other parameters, the leakage inductance can then beexpressed as a function of the area product

$$l_w = \left[\frac{A_w A_c}{a_{c1} a_{c2} a_w}\right]^{0.25}$$
$$l_{\mathrm{TR}} = \mu_o N_1^2 k_a U \left[A_w A_c\right]^{0.25} \qquad (11)$$
$$U = \frac{2(a_{c1} + a_{c2} + 2a_w)}{a_w \left[a_{c1} a_{c2} a_w\right]^{0.25}}.$$

TABLE I:

GEOMETRICAL PARAMETERS FOR ETD AND PLANAR CORES

	a_w	a_{c1}	a_{c2}	S	U
ETD	0.27	0.47	0.47	38	22.2
Planar E+I	3.2	5.9	1.25	58	3.8

It had been established in [1] and [4] that $L_{ito1} = l_{TR}/k$.Therefore, it is now possible to deduce an expression of therelative current ripple from (3)

$$\frac{\Delta i_{ito}}{I_{ito}} = \frac{[kD - q + 1]\,[q - kD]}{1 - D} \frac{V_{\mathrm{in}}}{I_{ito} k \mu_o n_1^2 k_a U \left[A_w A_c\right]^{0.25} F}. \qquad (12)$$

Finally, the proportion of the windowheight required to obtaina given value of the relative current ripple is

$$k_a = \frac{[kD - q + 1]\,[q - kD]}{1 - D} \frac{V_{\mathrm{in}}}{I_{ito} k \mu_o n_1^2 U \left[A_w A_c\right]^{0.25} F} \frac{I_{ito}}{\Delta i_{ito}}. \qquad (13)$$

The term k_a has strictly the same impact as the windingfactors $K_{w1,2}$. Consequently, accounting for the current ripplein the resolution of (9) can be made by replacing

$$K_{w1} \quad \text{by} \quad \frac{K_{w1}}{1 - k_a} \quad \text{and} \quad K_{w2} \quad \text{by} \quad \frac{K_{w2}}{1 - k_a}.$$

The flow chart of Fig. 12 shows the design process. A zerosearch of $G(A_cA_w)$ (9) is achieved, the variable being A_cA_w .For each iteration of the zero-search algorithm, $\Delta B_M(A_cA_w)$,then $J_{RMS}(A_cA_w)$, and then$G(A_cA_w)$ are calculated. The convergenceis reached when $G(A_cA_w) = 0$.

The resolution directly gives the core dimension in the chosenshape, according to the chosen thermal conditions (thermalexchange coefficient), but it probably does not exist because thedimensions vary continuously in the resolution, whereas onlya few cores exist in the real world. Nevertheless, an accuraterange of volume and characteristics is directly identified.The formulation can also be appliedin the other way bysetting A_wA_c as an input datum. For the resolution of (9), thevarying parameter becomes the frequency F but the process issimilar.

V. EXAMPLE OF ICT DESIGN RESULTS

The aim of this last section is to emphasize the requirementsof the ICT topology concerning the switching frequency and thenumber of cells by using a particular design case. The chosenspecifications, 28 V/10 kW, correspond to low input voltage–high power and are representative ofdc–dc embedded converterconnected to low-voltage networks, fuel cells, supercapacitors,etc.

The magnetic configurations considered in the design exampleare the planar E+I with stacked winding and the ETDwith concentric-stacked windings. Table I gives the geometricalcharacteristics of both families (average values), as well as thecorresponding coefficients S (thermal exchange) and$U$ (leakageinductance).The respective values of S and U confirm, on the one hand,that planar cores are a good solution to obtain good thermal

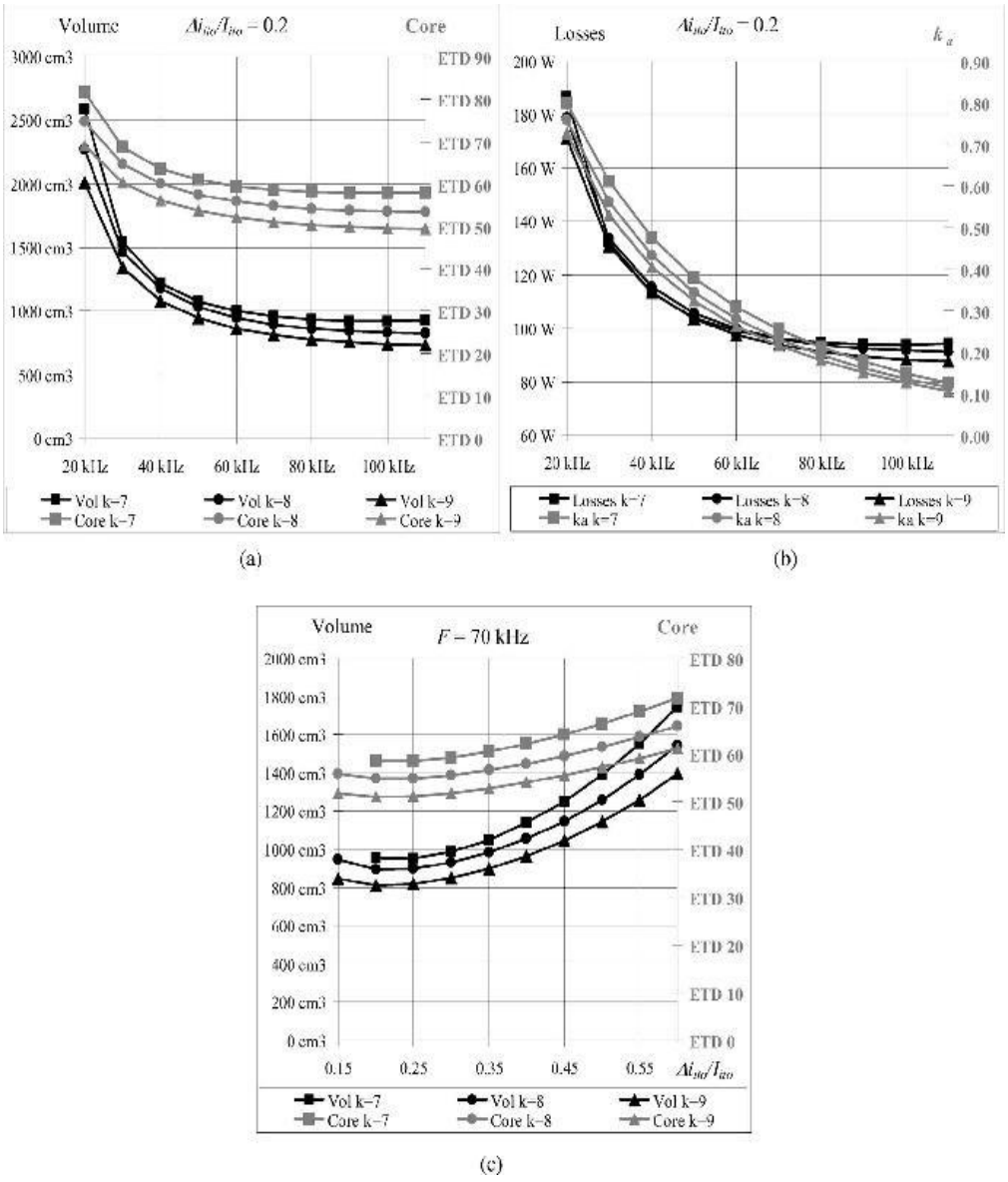

Fig. 13. ETD core results. (a) Volume versus frequency for ETD core. (b) Losses and interwinding space versus frequency for ETD core. (c) Volume versus relative current ripple for ETD core.

exchange and low leakages, which is not new, and on the other hand, that ETD cores will provide higher leakage inductances that at first sight seem preferable for ICT.

From these general specifications and by considering the topology of Fig. 3, different designs have been tested, in the 20–100 kHz frequency range with the number of cells k vary-ing between 6 and 10. In all cases, a temperature increase of 60 °C, a thermal exchange coefficient H of 15 °C/W/m^2 , and a transformer ratio of 1:12 have been fixed. Because of the low input voltage, the influence of connections has been taken into account. Indeed, the leakage inductance values required to limitthe ripple current on the primary side are around a few 10 nH. The parasitic inductance values of the connections are typically in this range and contribute to reduce the current ripple. There-fore, an additional inductance is introduced in the design of which the value is 1 μH/m × [core width], the core width being the minimal length to interconnect two adjacent cells.

For the ETD core shape, the best results have been obtained with values of the relative current ripple $\Delta i_{ito}/i_{ito}$ close to 20%, and with value of k from 7 to 9. They are summarized by the curves of Fig. 13(a) and (b). The ETD core shape al-lows getting lower relative current ripples (from 10%) but the

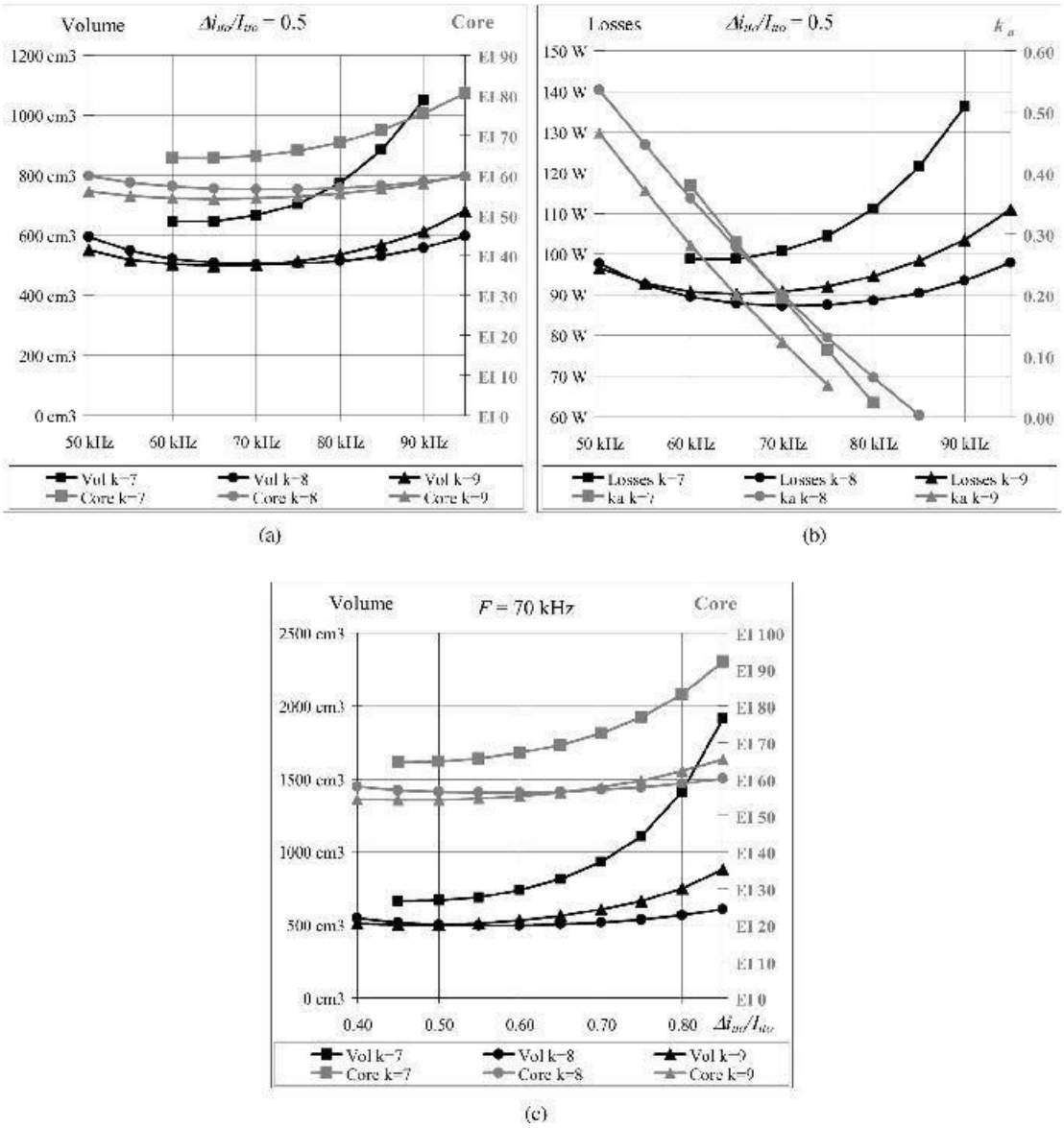

Fig. 14. EI Planar core results. (a) Volume versus frequency for planar core. (b) Losses and interwinding space versus frequency for planar core. (c) Volume versus relative current ripple for planar core.

optimum volumes are found around values of 20%–25% for number of cells higher than 6. This fact is illustrated by Fig. 13(c), which gives the volume evolution versus the cur-rent ripple, F= 70 kHz. The result is the same in any part of the frequency range. Concerning the value of k, under 7, the values of the relative current ripple cannot be limited, and for k higher than 9, the main characteristics, total volume, and losses, are not improved, whereas the complexity increases.

The first graph of Fig. 13 shows the evolution of the total vol-ume (k transformers) as the characteristic dimension of one of the transformer, classically the width of the core, versus the fre-quency. It varies continuously because of the homothetic design method, but it can be observed that standard cores ETD 54 or ETD 59 can be used on some parts of the frequency range. Thesecond graph gives the total losses as the relative interwinding space needed to reach the 20% value of the relative current rip-ple. The loss values are classical, around 1% of the total power and the values of interwinding space become realistic from 50 kHz. As can be seen in the different curves, in the ETD configuration, the number of cells has no significant impact on the global characteristics. Nevertheless, associated with the fre-quency parameter, it allows getting design results with standard cores.

For the planar shape, the design is more critical, because of the lower value of the leakage factor U . Then, to find design solutions with the same k values, the range of the relative current ripple has to be higher than 0.4. The best results are shown in Fig. 14(a) and (b) with a relative current ripple equal to 50%

which constitutes an optimal value in that case, as shown inFig. 14(c).

The planar solutions are considerably smaller than the ETDones, because of the better exchange coefficient, but the lossesare quite similar. The optimum value of the number of cells iseight, with lower volume and losses. In this case, the influenceof frequency is low. The calculated theoretical cores are veryclose to the standard core EI 58.

The two solutions are quite similar with respect to losses andthe frequency/number of cells requirement. The ETD optionleads to a higher volume but the lower value of the current ripple

has to be considered. That characteristic improves the operatingcondition of the semiconductor devices by reducing the maximalcurrent. A more advanced comparison would require designingall the converter parts to determine which design gives the bestoverall performance. However that may be, these results allowdefining the typical design domain of ICTs dedicated to multicellflyback converters and demonstrate their potential with a specificpower that reaches 20 kW/l (10 kW/500 cm^3) in the present case.

VI. Experimental Results

The previous results are currently applied to the design of a 28 V/10 kW prototype that will use the planar configuration with eight cells. In a first step, an ICT cell has been realized and characterized to validate the design process.

A. Transformer Specifications

The design of Fig. 14(a) with a switching frequency of 60 kHz and k_a= 0.8 has been chosen. The core is an EI 58 planar. The main parameters are given in Table II.

B. Realization

The primary conductor is stamped out in a copper sheet. It is designed as a short circuit to easily characterize the winding loss (see next section). The secondary conductors are realized on PCB. The insulating layers use a 25 μm Kapton sheet. Fig. 15 shows the different layers of the ICT cell.

C. Measurements of Winding Losses

To make the measurement of the winding losses with only one cell, a specific auxiliary test converter was realized. It was able to generate the different current components of Fig. 6 that were successively injected on the secondary side (see Fig. 16), the primary being in short circuit. For each component, the winding losses were deduced from a comparative measurement made with dc injection giving the same temperature increase.

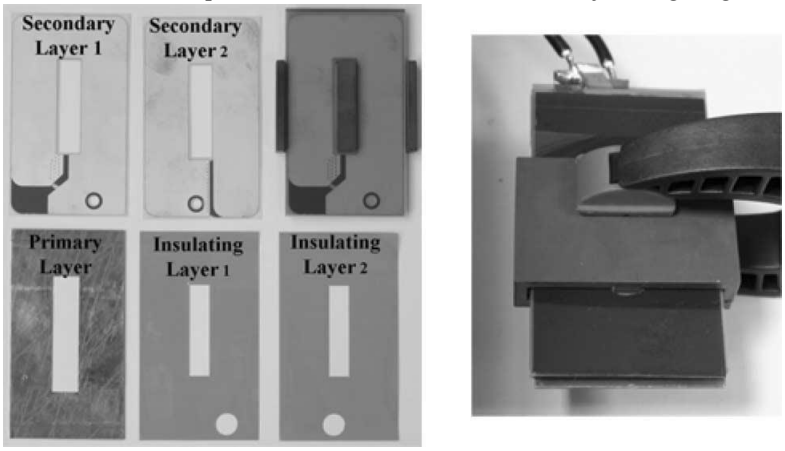

Fig. 15. Realization of the ICT cell.

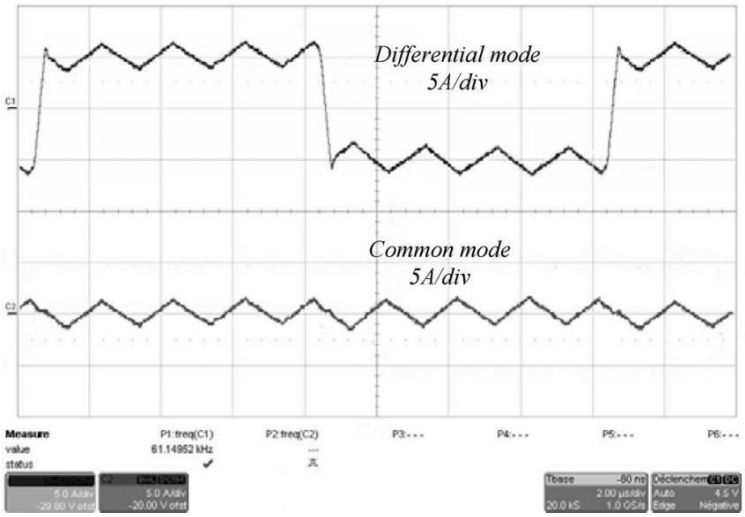

Fig. 16. Oscillogram of the current components

For the nominal power (1250 W), the results are the following.

1) Losses because of the ac differential mode: 5 W (ΔT= 28 °C).
2) Losses because of the ac common mode: 1.1 W.
3) Losses because of the dc mode: 2.8 W.

The total value of the measured winding losses is 8.9 W. This result is close to the theoretical one (8.47 W). The temperature increase (28 °C) obtained for the differential mode with 5 W, is in accordance with the theoretical design giving ΔT= 60 °C for total losses equal to 11.17 W. The accuracy of the design method is confirmed.

VII. CONCLUSION

This paper has shown the main design features of the iso-lated ICTs dedicated to the ICT flyback converter, an origi-nal and promising topology recently proposed by the authors. The isolated ICT is unusual for two reasons: first, the winding current shapes are particular, and second, the magnetic energy storage being provided by the leakages inductances has to be controlled. A 2-D model has been established to calculate the winding losses, and a design method, based on the area product calculation, has been developed to take into account the winding loss model and the estimation of the interwinding space required to adjust the leakage inductances. Then, this design method was applied to a typical case, with a low input voltage and highpower. In this field, the ICT flyback converter is a good candi-date. The results show the impact of the magnetic core shapes and of the number of cells. They confirm the good potential of the ICT flyback converter as well as the relevance of the method to design this multiparametric topology.

REFERENCES

[1] F. Forest, T. Meynard, E. Laboure, V. Costan, and J.-J. Huselstein, "A multi-cell interleaved flyback using intercell transformers," *IEEE Trans.Power Electron.*, vol. 22, no. 5, pp. 1662–1671, Sep. 2007.
[2] I. G. Park and S. I. Kim, "Modeling and analysis of multi-interphase transformers for connecting power converters in parallel," in *Proc. PowerElectron. Spec. Conf. 1997*, vol. 2, pp. 1164–1170.
[3] T. Meynard, F. Forest, E. Laboure,´ V. Costan, A. Cuniere,` and E. Sarraute, "Monolithic magnetic couplers for interleaved converters with high number of cells," presented at the IEEE CIPS Conf., New York, 2006.
[4] F. Forest, T. Meynard, E. Laboure,´ V. Costan, A. Cuniere,` and T. Martire,´ "Optimization of the supply voltage system in interleaved converters using intercell transformers," *IEEE Trans. Power Electron.*, vol. 22, no. 3, pp. 934–942, May 2007.
[5] P.-L. Wong, P. Xu, B. Yang, and F. C. Lee, "Performance improvements of interleaving VRMs with coupling inductors," *IEEE Trans. PowerElectron.*, vol. 16, no. 4, pp. 499–507, Jul. 2001.
[6] P. Zumel, O. Garcia, J. A. Cobos, and J. Uceda, "Magnetic integration for interleaved converters," in *Proc. Appl. Power Electron. Conf. 2003*, vol. 2, pp. 1143–1149.
[7] L.-P. Wong, D. K.-W. Cheng, M. H. L. Chow, and Y.-S. Lee, "Interleaved three-phase forward converter using integrated transformer," *IEEE Trans.Ind. Electron.*, vol. 52, no. 5, pp. 1246–1260, Oct. 2005.
[8] J. Li, C. R. Sullivan, and A. Schultz, "Coupled inductors design optimiza-tion for fast-response low-voltage DC-DC converters," in *Proc. IEEEAppl. Power Electron. Conf. 2002*, vol. 2, pp. 817–823.
[9] J. Li, A. Stratakos, A. Schultz, and C. R. Sullivan, "Using coupled in-ductors to enhance transient performance of multi-phase buck convert-ers," in *Proc. IEEE Appl. Power Electron. Conf. 2004*, vol. 2, pp. 1289– 1293.
[10] P. Zumel, O. Garcia, J. A. Cobos, and J. Uceda, "Tight magnetic coupling in multiphase interleaved converters based on simple transformers," in *Proc. IEEE Appl. Power Electron. Conf. 2005*, vol. 1, pp. 385–391.
[11] J. Czogalla, J. Li, and C. R. Sullivan, "Automotive application of multi-phase coupled inductor DC-DC converter," in *Proc. Ind. Appl. Soc. 2003*, vol. 3, pp. 1524–1529.

[12] P. Dowell, "Effects of eddy currents in transformer windings," in *Proc.Inst. Electr. Eng.*, vol. 113, no. 8, pp. 1387–1394, Aug. 1966.
[13] J. A. Ferreira, "Improved analytical modeling of conductive losses in magnetic component," *IEEE Trans. Magn.*, vol. 9, no. 1, pp. 127–131, Jan. 1994.
[14] J.-P. Keradec, B. Cogitore, and F. Blache, "Power transfer in two-winding transformer: From 1D propagation to an equivalent circuit," *IEEE Trans.Magn.*, vol. 32, no. 1, pp. 274–280, Jan. 1996.
[15] F. Forest, E. Laboure,´ T. Meynard, and M. Arab, "Analytic design method based on homothetic shape of magnetic cores for high frequency trans-formers," *IEEE Trans. Power Electron.*, vol. 22, no. 5, pp. 2070–2080, Sep. 2007.
[16] H. Njiende, N. Frohleke,¨ and J. Bocker,¨ "Optimized size design of inte-grated magnetic component using area product approach," presented at the CD-ROM EPE Conf., Dresden, Germany, 2005.
[17] G. Hurley, W. H. Wolfle,¨ and J. G. Breslin, "Optimized transformer design: Inclusive of high frequency effects," *IEEE Trans. Power Electron.*, vol. 13, no. 4, pp. 651–659, Jul. 1998.
[18] R. Petkov, "Optimum design of high-power high frequency transformer," *IEEE Trans. Power Electron.*, vol. 11, no. 1, pp. 33–42, Jan. 1996.
[19] J. T. Strydom and J. D. Van Wyk, "Electromagnetic design optimization tool for resonant integrated spiral planar power passives $(ISP)^3$," *IEEETrans. Power Electron.*, vol. 20, no. 4, pp. 743–753, Jul. 2005.
[20] G. Hurley, W. H. Wolfle,¨ and J. G. Breslin, "Optimized transformer design: Inclusive of high frequency effects," *IEEE Trans. Power Electron.*, vol. 13, no. 4, pp. 651–659, Jul. 1998.